

INSTABILITY CHARACTERISTICS OF SHOCK WAVES AHEAD OF A HEMISPHERICAL SHELL AT SUPERSONIC SPEEDS

Toshiharu Mizukaki*, Naofumi Kawamura*

***Dept. of Aeronautics and Astronautics, School of Engineering, Tokai University**
mizukaki@keyaki.cc.u-tokai.ac.jp; BMJM007@mail.tokai-u.jp

Abstract

To visualize the initiation of shockwave vibrations in front of a solid hemisphere model that had a diameter of 86 mm and thickness of 3 mm, a supersonic-wind-tunnel experiment was conducted. A schlieren system with a high-speed camera that had maximum frame rate of 100,000 frame-per-seconds, was used as an image-recording device. Shock waves behavior at Mach number 2.0, 3.0, 3.5, and 4.0 were examined. Shock vibration ahead of the model was observed at Mach numbers above 3.0. A hypothesis of the primary reason of shock instability and large deformation by the interaction between the detached shock wave and vortices which were emerged from inside of the model, based on the time-resolved images, was proposed. The mechanism of shock instability ahead of a hemisphere model would be applied to suppress and diminish deformation of supersonic parachute for planetary exploration.

1 Introduction

Re-entry and planetary entry of space vehicles have been widely conducted since 1960s. Parachute has been employed as deceleration device for the vehicles because its lightweight and easy stowing [1][2]. The parachute would be deployed at supersonic speed although a space vehicle would be decelerated by drag force after entering atmosphere of a planet. In 1960s and 1970s, experimental studies on behavior of supersonic parachutes were conducted with real parachutes made of fabric [3-12]. In these experiments, parachutes were destructed by fatigue shortly after deployment [13]. To reveal the mechanism of destruction of

parachutes, flow visualization around parachutes were widely conducted by researchers. Resultant images suspected that shock vibration ahead of parachutes strongly related with destructive deformation. In 1960s, imaging device had insufficient specification to obtain time-resolved-sequential-visualized images to reveal process of the destruction, although assumption had been proposed. Since 1990s, research interest has been arisen on re-entry and planetary exploration to the Mars again. Detailed experiments on shock instability ahead of a hemispherical shell model reported. Hiraki et al. [14] have reported on a shock wave oscillation ahead of a hemisphere model made of stainless steel, by using spark schlieren system, which allows one to obtain instantaneous-visualized images of high-speed phenomena. The research has revealed that frequency of oscillation of detached shock ahead of the model was 800 Hz in Mach 3.0 flow. The research also has shown the time history of pressure distribution on inside wall of the model. Takakura et al. [15] had numerically examined bow shock oscillation ahead of a 2-D model, which was an open-rectangular toward upstream, by WENO scheme with high-spatial resolution. The research clearly showed that generated vortices at edges of the model went upstream through subsonic region and interfered bow shock, at Mach 4.0.

In this paper, flow visualization with schlieren method combined with a high-speed video camera was conducted to evaluate shock-vortex interaction ahead of a hemispherical shell model in supersonic flows. A simplified parachute model, a hemispherical shell, made of stainless steel, was examined for flow visualization. A hypothesis on destructive-shock-deformation mechanism, based on time-

resolved-sequential images of oscillating detached shock, will be proposed.

2 Experimental Method

2.1 Hemispherical Shell Model

Figure 1 shows the hemispherical shell model which was a simplified parachute, examined in the paper. The model that was made of stainless steel, SUS304, had an outer diameter of 86 mm and a shell thickness of 3 mm. The outer side of the bottom of the model was connected and fixed at the tip of the sting in test section of supersonic-wind tunnel. The sting had a diameter of 30 mm. In the test section, the model had a blockage ratio of 1.6%.

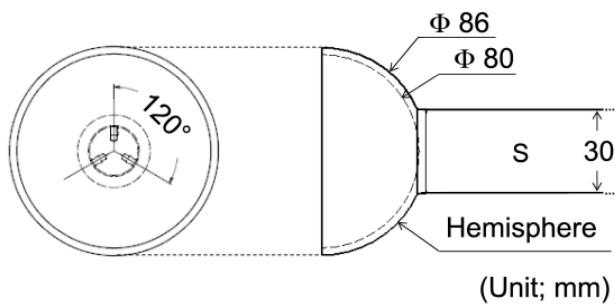


Fig.1 Schematic of the hemispherical shell model; S: sting.

2.2 Flow visualization

Figure 2 shows a schematic diagram of optical setup for flow visualization. A high-speed video camera was used as an image-recording device. The camera (frame rate; 100,000 Hz (max.), Vision Research Phantom V7.1) was installed in a schlieren system which schlieren mirror had a diameter of 0.6 m and a focal length of 5 m. The flow field around the model was recorded, as a image with 256 by 256 pixels, at every 200 μ s, and with 20 μ s exposure time. A continuous Xe lamp (500 W, Ushio Co., XB-10201AA-A) was used as a light source for visualization. The camera was manually triggered just after establishment of supersonic flow in the test section. Recording duration was about 20 seconds at maximum for the fastest framing rate during one test. A knife-edge was installed from vertical direction at the focal point to clearly

visualize density change through the shock waves ahead of the model.

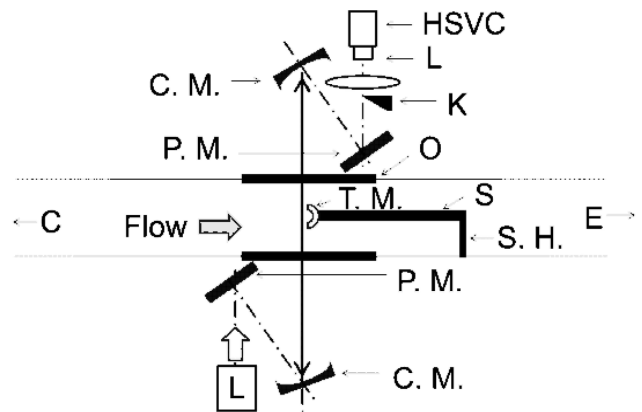


Fig. 2 Schematic diagram of Schlieren system combined with a high-speed video camera; HSVC, high-speed video camera; L, lens; K, knife edge; P.M., plane mirror; C.M., concave mirror; O, optical window; L, light source; C, plenum chamber; T.M., hemispherical shell model; S, sting; S.H., sting holder; E, ejector.

2.3 JAXA Supersonic Wind Tunnel

Experiments were conducted with a blow-down-type supersonic-wind-tunnel of ISAS, Japan Aerospace Exploration Agency (JAXA). The supersonic flow with Mach number up to four would be provided with the wind tunnel. The dimension of cross-section of the test section was 0.6-m by 0.6-m. Flow field around the model was visualized by schlieren system.

Table 1 shows the flow condition examined. For each conditions, the angle of attach was fixed at zero degree against the flow. Decision of value of the stagnation pressure P_0 and ejector pressure, based on the characteristic of the wind tunnel, were made so as to achieve the longest test duration for demanded Mach number. Shock wave vibration had been reported to be observed at Mach number over 3.0 in the literature [14][16]. Therefore, the experiment done here focused flow field at Mach number over 3.0. The run with Mach 2.0 was the control examination.

Table 1. Experimental conditions.

M	P_0	Ejector
(-)	(kPa)	(kPa)
2.0	210	None
3.0	440	None
3.5	406	392
4.0	510	490
4.0	593	392

3 Experimental Results and Discussion

Ahead of the model, shock wave vibration clearly appeared at the flow Mach number over 3.0 while only steady shock wave appeared at Mach number 2.0. Figure 3 shows a representative visualized flow field around the model in the supersonic flow at Mach 2.0. The image was recorded with a normal speed video camera (frame rate, 33 Hz).

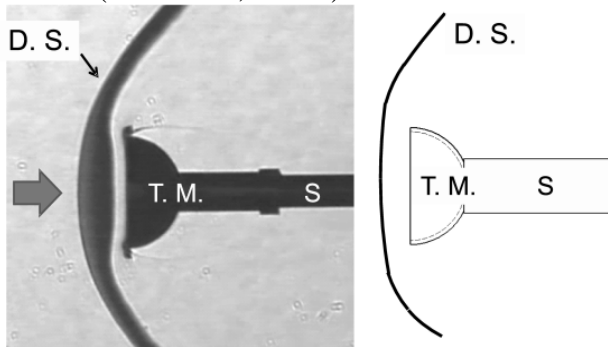


Fig. 3 Representative schlieren image of shock wave ahead of a hemispherical model at Mach 2.0 (flow from the left), D.S., detached shock wave; T.M., the hemispherical shell model; S, sting.

3.1 Process of Initiation of Shock Vibration

Figure 4 depicts the process of initiation of the shock oscillation and deformation ahead of the hemispherical shell model at Mach 3.0. Schlieren images and corresponding sketches are shown on the left-hand side and on the right-hand side, respectively. In fig. 4(a), the detached shock wave just before oscillating, which appeared ahead of the hemispherical shell model after flow establishment in the test section, is shown. Density disturbance, J, that emerged from inside the hemispherical shell model approached to the detached shock. The density disturbance collided with the detached shock about 400 μ s after its appearance. In fig. 4(b), deformation of the detached shock was initiated and oscillation expanded toward the radial direction. Vortices that were induced by the deformation appeared in the region between the detached shock and the hemispherical shell model. In fig. 4(c), the vortices moved from center part of the detached shock toward the edge of the hemispherical shell model and interfered with the edge. Interaction between the vortices and the edge produced the strong density disturbance that flew out from the

hemispherical shell model. When the density disturbance flew out, the distance between the detached shock and the edge was enlarged so that the disturbance emitted out. Immediately after the density disturbance emitted, the detached shock attached the edge. Then, large-deformation of the detached shock started.

Generally, Helmholtz resonator would be formed with an open-end cavity and flow coming into. Inside the cavity, standing wave with the wavelength determined by geometric condition, must be induced. In this experiment, the region between the hemispherical shell model and the detached shock would act as Helmholtz resonator because the region behind the detached shock was subsonic flow, which sound wave can propagate upstream.

From shock wave with curvature changing, vortex sheet is continuously generated into its flow field. In this experiment, the detached shock wave ahead of the edge of the hemispherical shell model was suspected to generate vortex sheet because of curvature changing. Therefore, vortices were supplied inside the cavity of the hemispherical shell model forming Helmholtz resonator.

The authors assume that the density disturbance discharged from the cavity of the hemispherical shell model, J in fig. 4 (a), is an intensified vortex by Helmholtz resonator. Helmholtz resonator reflected the generated vortices from the detached shock wave toward upstream with help of standing wave so that vortices hit the detached shock wave from downstream. The intensified vortex hitting the detached shock wave from downstream produced shock instability and finally initiated the large deformation.

3.2 Process of Succession of Shock Vibration

After the large-deformation of the detached shock wave was initiated, the distorted shock wave kept periodic motion for several seconds. A hypothesis on succession of cyclic interaction between the distorted shock wave and the flow emerging from cavity of the hemispherical shell model at Mach 3.0, based on the visualized images, is depicted in fig. 5. Schlieren images and corresponding sketches are shown on left-

hand and on right-hand side, respectively. At 200 μs after the initiation, shown in fig. 4(e), pressure wave emerged from the edge of the hemispherical shell model made the upper-side shock wave (1st D.S.) moved toward the upstream while the lower (2nd D.S.) moved into the cavity of the hemispherical shell model (fig. 5(a)). Consequently, the 2nd D.S. accelerated the air toward the bottom. The accelerated air produced flow along shell. Finally, the flow was discharged toward the detached shock wave. Then, the discharged flow made the shock stand-off distance from the upper edge of the hemispherical shell model enlarged (fig. 5(b)). After the discharging, the pressure inside the hemispherical shell model suspected to be decreased. Consequently, the detached shock moved toward and attached on the hemispherical shell model because of the resultant negative pressure (fig. 5(c)). The air inside the hemispherical shell model was accelerated again (fig. 5(d)). Finally, the oscillation with large deformation of the detached shock wave started and continued for a few seconds. In the experiment, the deformation was three-dimensional motion while the initiation process depicted above was described as two-dimensional phenomena. Because the emerged flow provided the momentum so that the detached-shock-wave system rotated, generation of the emerged flow was observed at the upper and the lower edge of the hemispherical shell model, one after the other.

Cyclic deformation that was described above stopped by itself after a few seconds. At every experiment with velocity above Mach 3.0, during test duration for one run, 30 seconds, the deformation of the detached shock was observed once or twice.

4 Conclusion

Hypotheses of the initiation and succession process of large-deformation of the detached shock waves ahead of a hemispherical shell model in steady supersonic flows, based on temporal visualized images, have been described. Flow visualization was conducted with a schlieren system combined with a high-speed video camera. The destructive deformation of the shock wave has been observed with velocity

above Mach 3.0 while steady shock wave has been observed with velocity of Mach 2.0. Because the paper has focused on observing time-resolved process of initiation of destructive large deformation of the detached shock wave ahead of a hemispherical shell model, quantitative measurement such as pressure measurement with pressure transducers has not been carried out. The deformation has been initiated by density disturbance such as a vortex emerged from inside of the hemispherical shell model. After the initiation, pressure disturbance has been amplified by the induced-oscillation of the shock waves. Pressure decreasing inside the hemispherical shell model has been induced when a large vortex blew out from the edge. Finally, destructive deformation of the shock waves appeared just after discharging of the vortex.

A hypothesis that the magnitude of pressure changes after discharging vortices would have an important roll on destructive deformation appearance, based on the time-resolved images on the interaction between the vortex and the shock waves, was proposed. The larger Mach number of steady flow would produce larger pressure disturbance inside the hemispherical shell model. The larger pressure disturbance would induce the vortex that would decrease the pressure inside the hemispherical shell model when the vortex was discharged toward outside flow. Also, the curvature of the edge of the hemispherical shell model would have an important roll on vortex size. The edge with small curvature would not let the vortex escape easily so that the magnitude of pressure changes inside the hemispherical shell model would be amplified.

To prevent shockwave vibrations, localized flow heating is supposed to be an effective method. Localized flow heating is an energy addition that is able to decrease drag around supersonic flying objects [17][18]. An electrode is installed at the upstream of the model and the flow is heated by an ark [17]. Accordingly, local sound speed increased. As a result, the shockwave ahead of the model would disappear. Thus, if localized flow heating is adopted, the origin of the vortices is removed. Furthermore, localized flow heating is able to erase the first

shockwave. Therefore, the detached shockwave that entered into the model also disappeared. As a result, shockwave vibrations were assumed not to have occurred. The adaptation of localized flow heating to shockwave vibrations needs to be investigated further.

Acknowledgment

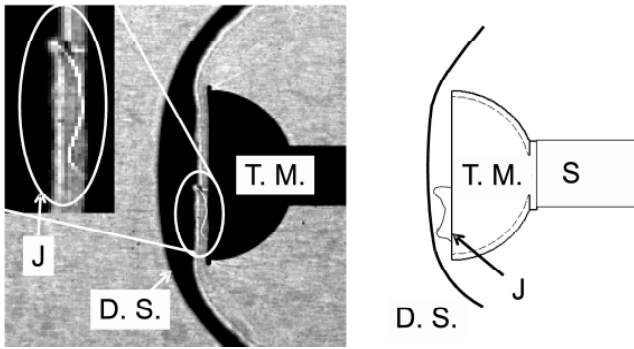
The authors would like to gratefully thank to Professor Takakura of the School of Engineering, Tokai University for her kind discussion on numerical analysis

Copyright Statement

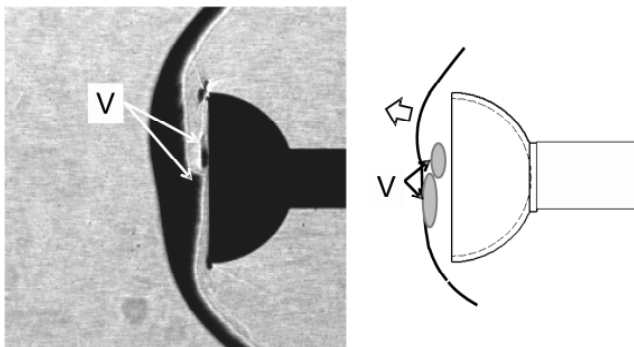
The authors confirm that they, and/or their company or organization, hold copyright on all of the original material included in this paper. The authors also confirm that they have obtained permission, from the copyright holder of any third party material included in this paper, to publish it as part of their paper. The authors confirm that they give permission, or have obtained permission from the copyright holder of this paper, for the publication and distribution of this paper as part of the ICAS2012 proceedings or as individual off-prints from the proceedings.

References

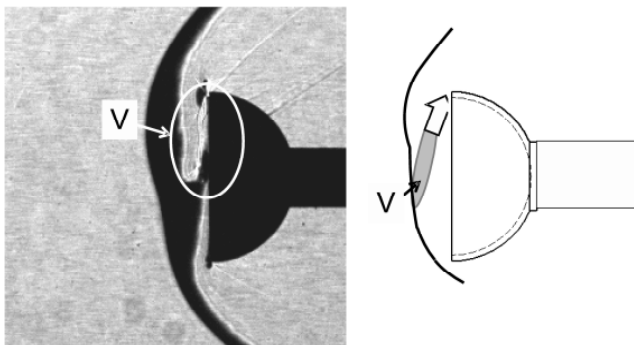
- [1] Underwood, J. C. and Sinclair, R. J., Wind tunnel testing of parachutes for Huygens probe, *The aeronautical J.*, pp. 357-364, 1997.
- [2] Murray, J. E. and Tartabini, P. V., Development of a Mars Airplane Entry, Descent, and Flight Trajectory, NASA Technical memorandum, NASA-TM-2001-209035, 2001.
- [3] Charczenko, N., Wind tunnel investigation of conventional types of parachute canopies in supersonic flow: NASA TMX-991, 1964.
- [4] Heinrich, H. G. and Haak, E. L., Stability and drag of parachutes with varying effective porosity, Air force flight development lab. tech. rept., AFFDL-TR-71-58, 1971.
- [5] Ewing, E. G., Bixby, H. W., and Knacke, T. W., Recovery system design guide, Air force flight development lab. tech. rept. AFFDL-TR-78-151, 1978.
- [6] Cockrell, D. J., The aerodynamics of parachutes, AGARD, AGARD-AG-295, 1987.
- [7] Heinrich, Helmut G., Some research effort related to problem of aerodynamic deceleration, Flight accessories laboratories for aeronautical systems division tech. note, WADD-TN-60-276, 1961.
- [8] Engstrom, B. A. and Meyer, R. A., Performance of trailing aerodynamic decelerators at high dynamic pressures part II, Cook research laboratories for Wright air development center tech. rept., WADC-TR-58-532, 1959.
- [9] Engstrom, B. A. and Lang, R. P., Performance of trailing aerodynamic decelerators at high dynamic pressures part V, Cook research laboratories for Wright air development division tech. rept., WADD-TR-58-284, 1961.
- [10] Berndt, R. J., Supersonic parachute research, Flight accessories lab. aeronautical systems division Tech. documentary rept., ASD-TDR-62-236.
- [11] Heinrich, H. G., Noreen, R. A., and Hedtke, J. C., Analysis of the opening dynamics of solid flat and ringslot parachute with supporting wind tunnel experiment, Air force flight development lab. tech. rept. AFFDL-TR-71-95, 1972.
- [12] Babish, C. A., The influence of aerodynamic delevelators on supersonic wakes: with an application of the gas hydraulic analogy, Air force flight dynamics lab. tech. rept., AFFDL-TR-72-54, 1972.
- [13] Heinrich, H. G., Aerodynamics of the supersonic guide surface parachute: *J. aircraft*, Vol. 3, No. 2, pp. 105-111, 1966.
- [14] Hiraki, K., Experimental study of aerodynamics about hemisphere model in supersonic flow, Tokyo University, 2006.
- [15] Shi, J. Zhang, Y. T., and Shu, C. W., Resolution of high order WENO schemes for complicated flow structures, *J. of computational physics*, Vol. 186, No. 2, pp. 690-696, 2003.
- [16] Takakura, Y., Hiraki, H. and Arai, N., On the Flow Fields around a Concave Body in Supersonic Flow: Proceedings of Symposium on Shock Waves in JAPAN 2008, 18-C-1-3, pp. 259-262, 2008.
- [17] Schulein, E. and Zheltovodov, A., Effect of steady flow heating by arc discharge upstream of non-slender bodies, *Shock Waves*, Vol. 2, No. 4, pp. 383-396, 2011.
- [18] Anderson, K. and Knight, D. D., Interaction of heated filaments with a blunt cylinder in supersonic flow: *Shock Waves*, Vol. 21, No. 2, pp. 149-161, 2001.



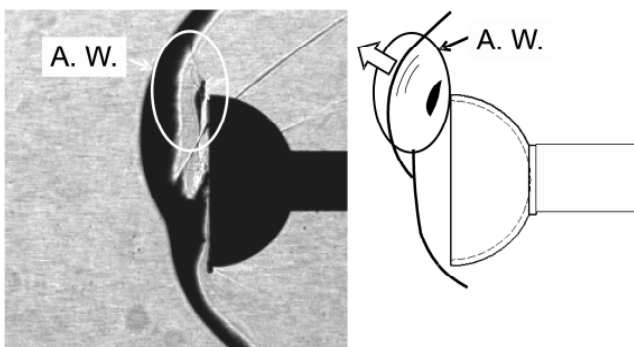
(a) $t = t_0$.



(b) $t = t_0 + 6.2$ s.

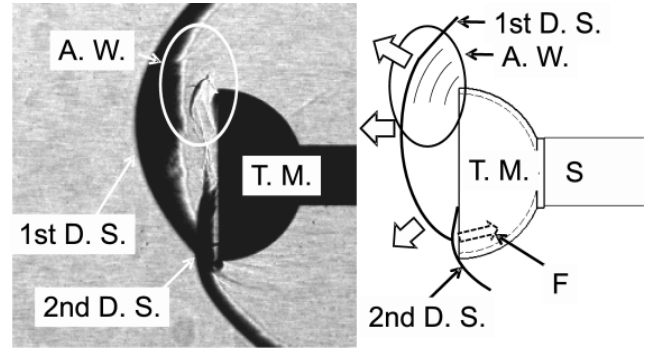


(c) $t = t_1 + 1.2$ ms.

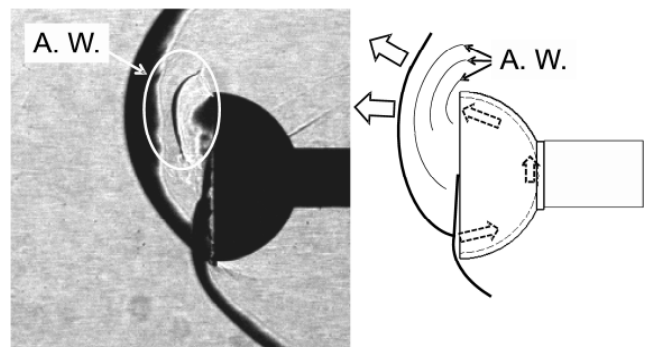


(d) $t = t_1 + 1.4$ ms.

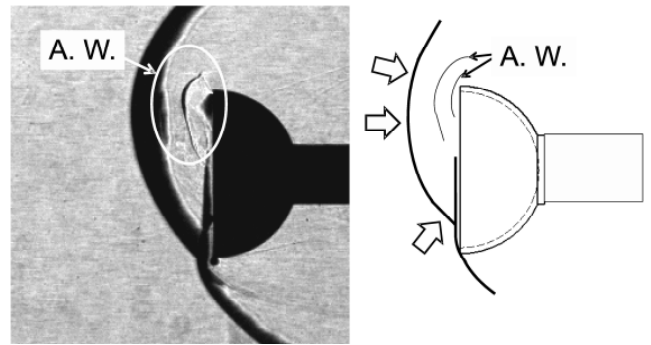
Fig. 4 Time-resolved Schlieren images of the initiation process of large deformation of the shock wave ahead of a hemispherical shell model in Mach 3.0 flow (flow from the left); T.M., hemispherical shell model; D.S., detached shock; S, sting; J, density disturbances; A.W., acoustic waves.



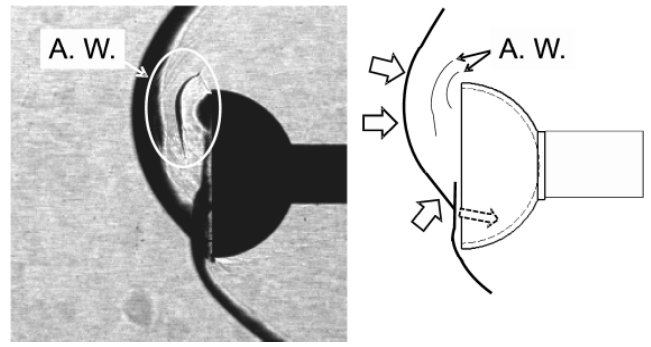
(a) $t = t_1 + 1.4$ ms.



(b) $t = t_1 + 1.6$ ms.



(c) $t = t_1 + 1.8$ ms.



(d) $t = t_1 + 2.0$ ms.

Fig. 5 Time-resolved Schlieren images of the succession process of large deformation of the shock wave ahead of a hemispherical shell model in Mach 3.0 flow (flow from the left); T.M., hemispherical shell model; D.S., detached shock; S, sting; J, density disturbances; A.W., acoustic waves.